Tradeoffs in bacterial physiology determine the efficiency of antibiotic killing

Anat Bren*, David S. Glass*, Yael Korem Kohanim, Avi Mayo, Uri Alon
Department of Molecular Cell Biology, Weizmann Institute of Science, Rehovot, Israel

Abstract

Antibiotics can kill or stop the growth of bacteria, and their effectiveness depends on many factors. It is important to understand the relation between bacterial physiology, the environment and antibiotic action. While many of the mechanistic details of antibiotic action are known, the connection between death rate and bacterial physiology is poorly understood. Death rate in antibiotics has often been shown to rise linearly with growth rate; however, it remains unclear how environmental factors, in concert with whole-cell physiological properties, affect bactericidal activity. To address this, we developed a high-throughput assay to precisely measure antibiotic-mediated bacterial death. We found that death rate is linear in growth rate only under certain conditions and deviates significantly from linearity in stressful growth environments: stressors lower the death rate compared to a non-stressed environment with the same growth rate. To understand the role of stress, we developed a mathematical model of bacterial death based on resource allocation that takes into account a newly defined stress-response sector; we identify this sector using RNAseq. Our model accurately predicts the death rate and minimal inhibitory concentration of antibiotics across a wide range of conditions, including a previously unknown increase in the stress response and protection from death at very low levels of cAMP. The present death-growth model suggests conditions that may improve antibiotic efficacy.

Introduction

The first antibiotic was discovered over 100 years ago [1]. Since then, many antibiotics that either kill the bacteria (bactericidal) or primarily inhibit their growth (bacteriostatic) have been discovered [2]. The direct interactions and proximal mechanisms of action have been elucidated for many antibiotics. However, the connection between the molecular mechanism of action and the physiological state of the bacterium (e.g., growth rate, proteomic profile) that ultimately leads to death remains poorly understood [2–4]. Understanding how bacteria deal with antibiotics is particularly relevant due to increasing issues of resistance mutations[5–7]. Another concern in antibiotic treatment is tolerance, a natural ability to survive in antibiotics that does not involve genetic changes [8]. Tolerance is known to depend on the bacterial growth environment [8–10], but its connection to environment and physiological state is poorly understood. Because of this clinical importance, many studies have approached antibiotic efficacy from the perspective of outcome (i.e., bacterial death) rather than the

physiological state of the bacterium (see [2] for a recent review). In this paper, we focus on the connection between death rate and physiological state as relates to tolerance.

Previous studies found linear relationships between growth rate or metabolic state and death rate due either to bactericidal antibiotic [11–17] or to starvation [18]. In contrast to these simple linear relations, combinatorial treatments have counterintuitive effects (see [19]for a recent review). For instance, bacteriostatic antibiotics protect against death due to bactericidal antibiotics [19] and anti-ribosomal antibiotics protect against anti-DNA antibiotic [20]. Additionally, it has been found that a bacteriostatic antibiotic (trimethoprim) increases the stress response and protects bacteria against acid [21]. Moreover, an active starvation response as well as other stressors were found to protect bacteria from antibiotics [9,10,23,24]. It is thus reasonable to expect that the connection between growth rate and death rate is more complex than a simple linear function of growth rate and may be dependent on the environment and the physiological state of the cell.

Unlike the death rate, the growth rate has been extensively studied in terms of physiology, revealing simple growth laws [24–28]. An early example of a growth law is the linear increase of growth rate with ribosomal content [25] (the basis of an "R sector" in later terminology [28]). This simple growth law has proven impressively capable of predicting bacterial growth rates across a wide range of environmental conditions, despite the thousands of underlying molecular reactions [24,25,28]. More detailed yet still coarse-grained models extended the growth laws to predict growth rate as a function of multiple internal proteomic sectors, each representing large groups of genes with similar behavior under corresponding resource limitations [29–31]. For example, the "C sector" represents genes which are upregulated under carbon limitation [29,32,33].

One attempt to relate resource allocation to death proposed that investment in maintenance prolongs survival during starvation [18]. We hypothesized that a generalized resource-allocation model, which takes into account tradeoffs between sectors due to limited cell resources, could connect environmental conditions, internal bacterial physiology and antibiotic killing rates. To build and test such a model requires accurate measurement of death rates in many conditions.

In this paper, we develop a high-throughput method to measure bactericidal death rates in a variety of conditions. We find that the death rate does not depend on growth rate alone, but also on the details of the environment. Stressful environments protect from bactericidal killing relative to non-stressed environments with the same growth rate. We hypothesized that stressful environments activate a cellular physiological program that helps bacteria to deal with antibiotic damage [34]. To test this, we used this data to develop a mathematical model that can quantitatively recapitulate death rates from given environmental conditions, based on tradeoffs in the allocation of resources to growth-related and stress-related proteomic sectors. We confirm the existence of such a stress sector, the S sector, using RNA sequencing, and quantitatively validate the model using C (carbon), S (stress), and R (ribosomal) sector sizes in various conditions. By directly manipulating the C sector via cAMP, we find a surprising decrease in death at low cAMP, which is quantitatively predicted by the model. Finally, we relate growth and death rates to clinically relevant quantities such as tolerance and minimal inhibitory concentration (MIC) and discuss conditions that may improve antibiotic killing of bacteria.

Results

High throughput assay of bacterial death rates

Bacterial death rates are classically measured by determining death rate via the colony-forming unit (CFU) assay. This assay estimates the number of viable bacteria remaining after various times in a damaging treatment by counting colonies that grow after plating on permissive agar media. This method is labor-intensive and limited in throughput. High-throughput measurements of decreasing optical density (OD) [12] or of minimal duration of killing (MDK) [35] are either limited to specific antibiotics that disrupt cell integrity (e.g., ampicillin) or yield limited time-course information. Single-cell tracking of death via microfluidics [36] is not easily scaled to measurement in many conditions. Overall, there is a lack of robust, high-throughput methods to measure death curves.

Here, we developed such an automated, high-throughput assay to measure death rates in 96-well plates in a robotic system (details in Fig 1 and Methods). In short, we measured the surviving fraction of cells as a function of antibiotic challenge duration. The robotic system enabled us to run a reverse time course with antibiotic introduced to exponentially growing cultures at a consistent OD (Fig. 1A, Fig. S1). Following the start-growth-time method of Hazan, *et al*., we estimated surviving cell numbers by measuring the time τ for a diluted, treated culture to reach a measurable OD threshold in permissive (minimal glucose) media (Fig. 1B)[37]. Fewer live cells growing exponentially will take longer to reach the threshold and thus represent lower percent survival, which we quantified by comparison to delays τ in untreated, diluted cultures (Fig. 1C). From percent survival in a range of antibiotic treatment durations, we obtained a survival curve and fit it to a Weibull survival function coupled to exponential growth (see Methods). Note that in some conditions we observed an initial increase in the number of viable bacteria, reflecting that bacteria at first grew faster than they died (Fig. S2), as has been observed previously [12]. We defined death rate as $1/t_{90}$, the inverse of time to reach 10% survival of the initial population (Fig. 1D, Fig. S3, Methods). We validated this approach by comparison to the CFU method and found excellent agreement (Fig. S4). Overall, the protocol provided throughput of 8 challenge-duration timepoints at 0.5 - 1 h resolution for 8 growth conditions in a two-day experiment (see Fig. S2 for all death curves obtained in this study).

Death rate depends on both growth rate and physiological stress

Using this assay, we explored the relation between growth and death rates of *E. coli* NCM3722 under various physiological conditions. As a challenge, we used 10µg/ml of the bactericidal antibiotic nalidixic acid, which interferes with DNA gyrase [38]. We used multiple growth conditions and evaluated the growth rate in each in the absence of the antibiotic challenge. First, we studied the effect of various carbon sources in a minimal growth medium. We find, in agreement with previous studies, that the lower the growth rate, the lower the death rate. Death rate in glucose, which supported the fastest growth, was the highest; death rate was lowest in the poorest carbon sources, galactose, and mannose (blue dots, Fig. 2A)

We next used glucose as a carbon source and reduced the growth rate by applying stress conditions: varying levels of either NaCl or the bacteriostatic antibiotic trimethoprim (TMP). We found that the growth-death relation was steeper in stressors than in the carbon

sources. In other words, we found that the death rate is not only a function of growth rate, but depends on the environment, with stressful conditions providing dose-dependent protection from death (orange and green dots, Fig. 2A). For example, the death rate on mannose or galactose was ~2.5-fold higher than the death rate at a similar growth rate reached by 300mM NaCl or 0.2µg/ml TMP, with much steeper survival curves (Fig. 2A, B). At higher stress levels (400 mM NaCl, 500 mM NaCl, 0.5 µg/ml TMP), the bacteria did not die (no measurable decrease in survival within 16 h, see Fig. S5). In other words, bacteria under these conditions became completely tolerant to the applied antibiotic treatment.

Since the decrease in death is not due to genetic mutations, it is expected that higher antibiotic concentrations will lead to death. We can thus connect this tolerance-derived decrease in death rate to zero with another key concept in antibiotic treatment: MIC, the minimal concentration of antibiotic that leads to death. We thus expect that under these stress conditions, MIC will be higher than the concentration used in the death-measurement experiments (10 µg/mL). Confirming this prediction, we found that the MIC (determined from OD measurements, see Methods and Fig. S6) in the high-stress conditions with immeasurable death rate had MIC above 10 µg/mL (Fig. 2C).

Note that although the growth-death relation for NaCl and TMP are similar at 10µg/mL nalidixic acid (Fig 2A), the differing MIC for 500 mM NaCl and 0.5 µg/mL TMP (Fig. 2C) despite similar growth rates (see below) suggests that the physiological response to these two stresses may not be identical.

We conclude that death rate is not solely a function of growth rate. Antibiotic causes a higher death rate when applied to bacteria growing on a poor carbon source than when it is applied to bacteria with the same growth rate growing on a rich carbon source supplemented with stressors.

A resource allocation model can explain the observed growth-death data

We hypothesized that a resource-allocation model including a stress sector can explain the observed growth and death rates. We begin with the dependence of death rate on growth rate in different carbon sources, which we call the 'sugar line' (Fig. 2A, blue points). On the sugar line, the well-established resource allocation theory predicts that as more resources are dedicated to carbon catabolism (C sector), fewer resources are dedicated to building ribosomes (R sector), resulting in a correspondingly lower growth rate[29,32,33]. One may assume that under these conditions the death rate increases in direct correlation to growth rate due to increased production of damage in line with previous descriptions[11,15] (e.g., nalidixic acid affects DNA gyrase, which introduces DNA breaks during replication[39]).

In contrast, when growth rate is varied via the concentration of stressors with glucose as a carbon source, we expect the C sector to remain constant. We base this expectation on the fact that the carbon source remains unchanged and the stresses imposed are unrelated to metabolic constraints. Under stressors, we then predict that resources are redirected to a newly defined stress response sector (S sector) at the expense of the R sector. This increase in stress-related genes can provide protection against antibiotic damage, while decreasing growth rate, resulting in a 'stress curve' (Fig 2A, green and orange points). We assume that under the conditions we studied, changing resources are divided strictly into the R, C and S sectors, while other sectors remain unchanged.

Based on the above hypotheses, we developed a mathematical resource-allocation model, summarized by the following equations. First, the sum of all sectors equals one [28]:

Eq (1) $C + S + R = 1$,

where C, S, and R correspond to the carbon, stress, and ribosomal sectors, respectively, where we normalize out "constant resources" that do not depend on conditions used in this work. Second, the growth rate μ depends on the R sector, as described by the well-established linear growth law [25,28]:

Eq (2) $\mu = aR - b$,

where a is the ribosomal growth efficiency and b/a the ribosomal spare capacity. Thirdly, the death rate ρ increases with damage which is proportional to growth rate and reduced by a saturating function of the S sector, leading to the proposed death law:

Eq (3) $\rho = \rho_0 + \alpha(\mu - \mu_0) - \beta \frac{S - S_0}{k + S - S_0}$.

The parameters μ_0 and ρ_0 represent the baseline growth and death rates on glucose. α describes the decrease in death rate per decrease in growth rate. β represents the increased protection from death with increased S, saturating with a Michaelis-Menten parameter k. We assume that on the sugar line, which lacks stressors, S remains constant ($S = S_0$), while on the stress curve on glucose C remains constant ($C = C_0$).

Equations 1-3 provide a good fit to the present growth-death measurements (Fig. 3A, Table S2), providing estimates of the parameters α, β, μ_0 ρ_0, and $k \cdot a$, but leaving free the parameters C_0, S_0, a, and b that are needed to determine the absolute sector sizes. Notably, the value of k (Table S1) is comparable to S, resulting in a nonlinear stress curve.

The fits provide a one-to-one mapping from sector size (C, S) to growth and death rates (μ, ρ) and vice versa (see Methods). We show this in Fig. 3B, in which nearly horizontal lines depict constant S with varying levels of C, and nearly vertical curves depict constant C with varying S. This mapping then predicts the growth and death rates given any combination of carbon quality and environmental stress. For instance, acetate can serve as a carbon source, but also induces a stress response [41,42]. Indeed, we find that acetate lies between the sugar line and stress curve (Fig 3B), which we can use to predict the sizes of C and S in this condition. These predictions then imply an equivalent mixed condition of a sugar (other than glucose) with a certain concentration of stressor. Following the grid lines in Fig. 3B, we predicted acetate to have death and growth rates approximately equal those on growth on glycerol + ~230mM NaCl or glycerol + ~0.15µg/mL TMP. Indeed growth and death rates in glycerol +230mM NaCl are within measurement error of those in acetate. In glycerol+0.15µg/mL TMP growth rate matched that of acetate but death rate was higher, suggesting a synergistic interaction between TMP and glycerol (Fig. S7). This discrepancy also suggests that, as seen in the MIC data, NaCl and TMP impose a different stress response.

The resource allocation model accurately predicts MIC as a function of growth rate

The level of stress which leads to a zero death rate ($\rho = 0$), is precisely that condition with MIC equal to the concentration of nalidixic acid used in the death rate measurements (10 µg/mL). In order to predict the MIC in other conditions, we assume to a first-order approximation that the term in Eq. 3 that are unrelated to the S sector increase linearly with the concentration of nalidixic acid (i.e., $\alpha = \alpha_0(n - n_0)$ and $\rho_0 = \mu_{00}\alpha$, with some baseline

MIC in glucose n_0). From this we derive (Methods) that MIC (n) is inversely proportional to growth rate under stressors but is unchanged in carbon sources. To test this prediction, we measured MIC for all conditions in Fig. 2. We indeed find the MIC increases with decreasing growth under stress, but does not change with differing carbon source. We note that TMP and NaCl differ quantitatively in their MIC-growth rate relations. Accordingly, using the parameters from Fig. 3A, we fit the additional parameters μ_{00}, n_0, and two separate values of α_0 for TMP and NaCl. We find excellent agreement between the model prediction and the measurements (Table S2). Note that α_0 only appears in the MIC model as β/α_0, and so the difference between TMP and NaCl could be attributed just as well to a increase in the efficiency of damage removal ($\propto \beta$) as to decrease in damage accumulation ($\propto \alpha_0$).

Gene-expression measurements support the model's prediction of a sizable stress sector

A basic assumption of the proposed model is a sizable S sector, whose fraction of cellular resources at high stress is significant enough to lead to a decrease in the R sector and a corresponding decrease in growth rate.

To test this, we first used a strain deleted for the major stress response regulator RpoS[42] and measured the MIC for nalidixic acid. Under TMP-stressed conditions, MIC in the ΔrpoS strain was unaffected by TMP concentration (Fig. S8), in contrast to the wild type strain where MIC rose with TMP concentration. Since RpoS is known to control expression of many downstream genes [43], this finding suggests that a large number of genes are likely to be involved in the S sector.

MIC under NaCl stress in the ΔrpoS strain behaved similarly to the wild type strain (Fig. S8), perhaps due to differing regulatory mechanisms between the response to NaCl and TMP.

To examine the size and composition of the S sector in more detail, we performed RNA-Seq analysis on *E. coli* NCM3722 cultures grown in various carbon sources or in glucose with increasing concentrations of NaCl or TMP. We used two-stage coarse-graining, with a Gaussian mixture model to group genes into clusters and then grouped the clusters by increasing, decreasing, or insignificant Spearman correlation between cluster summed expression on growth rate (see Methods).

Based on this analysis, we defined the R sector as the clusters correlated with growth rate in at least one of the three sets of conditions (NaCl, TMP, or sugars) and not anticorrelated with growth rate in any of set (2392 genes). We defined the S sector as clusters anticorrelated with growth rate in NaCl or TMP but not in poor carbon (784 genes). The remaining clusters were defined as the C sector (1053 genes), which included clusters increasing in both poor carbon and NaCl. We note that the R sector in this definition includes the classic ribosomal R sector, and also includes all other non-ribosomal genes that rise with growth rate [44,45].

Enriched GO terms in these clusters (Fig. 3D, methods) match the expectation that C is catabolism-related, R is ribosomal and growth-related, and S genes are stress-related. The inferred S sector also included anabolic genes, presumably related to requirements for production of, for example, osmoprotectants. In accordance with the model assumptions, these results show that we could indeed identify a meaningful C sector that remains largely constant under stressful conditions (Fig 3E), and a meaningful S sector that remains largely

invariant to carbon source (Fig. 3F).

The R sector inferred here rises linearly with growth rate, as required from our sector definitions (Fig. 3G). However, the linear dependence differs between carbon sources and stressors. This difference may be due to a lower translation rate for R-sector genes under stress[46], so that more ribosomal mRNA is required to provide a consistent amount of ribosomal protein. The 'classic' ribosomal R sector, which relates strictly to ribosomal content, can be measured by total RNA, which is predominantly ribosomal RNA. Total RNA shows the expected growth law: a linear dependence on growth rate that is similar in poor carbon sources and in stressors (Fig. 3G inset).

Modulating cAMP revealed a death-growth relation with characteristics of both sugar and stress curves

Measuring death in addition to growth provides us with two distinct physiological outputs of bacterial behavior. Using our resource allocation model, we have directly related these measurements to two sectors, C and S (R following from Eq. 1), using a set of conditions in which either C or S was held constant. We wondered whether we could find a series of conditions that more smoothly interconvert C and S. To do so, we focused on cAMP, a small molecule that quantitatively modulates the C sector[30,32,33]. Experimentally, we can manipulate cAMP levels in a ΔcyaA ΔcpdA strain that cannot produce or degrade cAMP [30,32,33].

This manipulation results in a non-monotonic dependence of growth rate on cAMP levels, in which the maximal growth rate on glucose and corresponding cAMP concentration resemble growth of the wild-type strain on glucose [30,33](Fig. S9). Increasing cAMP above its optimal level reduces growth rate due to an increase in the C sector at the expense of the R sector[30,32,33]. Division of resources at cAMP below the optimal point is less clear. At such low cAMP, both the C and R sectors decrease, accompanied by a slight increase in anabolism (A sector) [30]. By measuring death in addition to growth, we hypothesized that we may find additional differences that distinguish the low-cAMP branch from the high-cAMP branch, reflected perhaps in an increased S sector in this regime. If so, we hypothesize that the death rate at cAMP levels below the growth optimum will be lower than the death rate for cAMP level above the optimum with a similar growth rate.

We performed the death-growth measurements (Figs. S10-S11) in the ΔcyaA ΔcpdA strain at various cAMP concentrations and found a continuous curve connecting two phenotypic branches (Fig. 4A): high cAMP ($\gtrsim 0.2$ mM) and low cAMP ($\lesssim 0.2$ mM). In effect, using two physiological measurements, we were able to differentiate between these two branches: the death rate-growth rate slope was higher at low cAMP than at high cAMP. This would have been impossible by measuring only growth rate (e.g., 0.05 mM cAMP and 1 mM cAMP both have growth rate $\approx$0.57 h^{-1} but differ more than 2-fold in death rate). Qualitatively, this seems to indicate that high cAMP behaves like the sugar line not only with respect to growth rate [33] but also with respect to death. In particular, death rate was above zero for all measured conditions, even with the growth rate reduced by ~60%. In contrast, low cAMP behaves more like the stress curve. Death at low cAMP reached zero with growth rate reduced by only ~30%.

For low cAMP, the MIC likewise increased with decreased cAMP in a dose-dependent manner. For high cAMP, MIC increases as well, but primarily at very high concentration of

cAMP ($\gtrsim 2.5$ mM), above the endogenous levels for the poorest carbon sources we measured [33,47] The MIC increase also matches a previous study in a knockout of the cAMP receptor, CRP[48].

Considering this finding in light of the model, low cAMP levels should increase the S sector. Such low levels may thus be interpreted by the cells as a stress signal. Very high levels of cAMP may similarly represent a stressful condition.

To determine whether our model quantitatively captures this behavior, we substituted into the model growth rate measurements as a function of cAMP and proteomic data from Kochanowski, *et al* [30] on the relation between the C sector and cAMP in a similar ΔcyaA ΔcpdA strain (see Methods). A fit of our model then nicely captures the non-monotonic behaviors of both death rates and MIC (Fig. 4A, B respectively, Table S2). These results suggest that low and high cAMP ranges are distinct physiological states. At high cAMP, primarily the C sector increases with decreased growth rate, while for low cAMP primarily the S sector increases with decreased growth, thereby providing protection from death. Thus, on the high cAMP branch, a tradeoff exists between C and R, while on the low cAMP branch a tradeoff exists between S and R.

Discussion

We developed a high-throughput assay for measuring bacterial death curves. Using this assay, we determined the relation between the growth rate in a given condition and the death rate in a subsequent antibiotic challenge. Death rate depended both on growth rate and growth condition. Stressful conditions protected from death when compared to no-stress conditions of equal growth rate, such as growth on a poor carbon source. Stress resulted in lower death rate and increased MIC. The quantitative relation between growth and death is captured by a resource allocation model, in which death is increased by growth-related damage and reduced by a protective stress sector. We identified this stress sector using RNA-Seq measurements. In line with the model, MIC increased when a stress regulator was knocked out, and protection from death was gained when manipulating the C-sector to low levels via exogenous cAMP.

Most of the work on bacterial growth laws has focused on growth rate, not on death rate. Growth laws are explained by resource allocation models that focus on the relation between proteome distribution and growth rate. These models define sectors by an increased expression of a group of genes needed to cope with a certain limitation at the expense of ribosomes [28–30]. Here, we find that resource allocation-based theory can also predict death rate when a newly defined stress sector is introduced.

These findings emphasize the need to define what conditions are considered stressful for bacteria and to quantitate the S sector to predict death rate. One of the stressors we used is the bacteriostatic antibiotic trimethoprim (TMP), which reduces growth rate in a dose-dependent manner[20]. Our results thus provide an explanation for the known antagonistic effect of bacteriostatic antibiotics on bactericidal action[19]: bacteriostatic antibiotics in general may raise a stress response and thereby reduce death by bactericidal antibiotics. An additional way to impose stress is starvation, known to provide tolerance and persistence to antibiotics while upregulating stress-gene expression[9,10,24,50]. It will be interesting to measure antibiotic-mediated death rates and the size of the S sector under starvation.

A molecule often associated with stress, mainly in the context of starvation, is ppGpp[50]. Increased ppGpp leads to increased tolerance and persistence (see [22] for a recent review). ppGpp indirectly increases RpoS [50], which is one way to increase the S sector. In this way, the proposed model fits with the ppGpp literature. The model leaves open the possibility that stressors may more generally affect the S sector without the involvement of ppGpp. Similarly, ppGpp may be involved in the effect of cAMP on the S sector.

In addition to the connection between growth conditions and death rate, the present findings highlight the importance of considering growth conditions when determining the MIC for a given antibiotic. An elevated MIC is usually considered a form of resistance, such as that caused by mutations. A raised MIC can also result from stressful growth conditions without mutations[23,51], in a manner captured quantitatively by our resource allocation model.

Clinically, our work suggests that in the variety of conditions in the body, bacteria may be tolerant and even (non-genetically) resistant to antibiotics compared to laboratory conditions. For example, some of the stress placed on bacteria by the immune system may counterintuitively inhibit the killing efficacy of antibiotics. This suggests possible targets for treatments. For instance, provision of inhibitors of alternative sigma factors together with antibiotics may inhibit stress sector expression and enhance antibiotic efficacy. We anticipate that quantitative understanding of the death-growth tradeoff in bacteria and its relation to stress may thus have clinical applications, and more generally may advance our understanding of tradeoffs in bacterial physiology.

References

1. Fleming, A. & Wright, A. E. On a remarkable bacteriolytic element found in tissues and secretions. *Proceedings of the Royal Society of London. Series B, Containing Papers of a Biological Character* **93**, 306–317 (1922).
2. Baquero, F. & Levin, B. R. Proximate and ultimate causes of the bactericidal action of antibiotics. *Nat Rev Microbiol* **19**, 123–132 (2021).
3. Kohanski, M. A., Dwyer, D. J. & Collins, J. J. How antibiotics kill bacteria: from targets to networks. *Nature Reviews Microbiology* **8**, 423–435 (2010).
4. Stokes, J. M., Lopatkin, A. J., Lobritz, M. A. & Collins, J. J. Bacterial Metabolism and Antibiotic Efficacy. *Cell Metabolism* (2019) doi:10.1016/j.cmet.2019.06.009.
5. Murray, C. J. *et al.* Global burden of bacterial antimicrobial resistance in 2019: a systematic analysis. *The Lancet* S0140673621027240 (2022) doi:10.1016/S0140-6736(21)02724-0.
6. Bhattarai, K., Bastola, R. & Baral, B. Antibiotic drug discovery: Challenges and perspectives in the light of emerging antibiotic resistance. in *Advances in Genetics* vol. 105 229–292 (Elsevier, 2020).
7. Courvalin, P. Why is antibiotic resistance a deadly emerging disease? *Clinical Microbiology and Infection* **22**, 405–407 (2016).
8. Brauner, A., Fridman, O., Gefen, O. & Balaban, N. Q. Distinguishing between resistance, tolerance and persistence to antibiotic treatment. *Nature Reviews Microbiology* **14**, 320–330 (2016).
9. Fung, D. K. C., Chan, E. W. C., Chin, M. L. & Chan, R. C. Y. Delineation of a Bacterial Starvation Stress Response Network Which Can Mediate Antibiotic Tolerance Development. *Antimicrobial Agents and Chemotherapy* **54**, 1082–1093 (2010).
10. Nguyen, D. *et al.* Active Starvation Responses Mediate Antibiotic Tolerance in Biofilms and Nutrient-Limited Bacteria. *Science* **334**, 982–986 (2011).
11. Tuomanen, E., Cozens, R., Tosch, W., Zak, O. & Tomasz, A. The rate of killing of Escherichia coli byβ-lactam antibiotics is strictly proportional to the rate of bacterial growth. *Microbiology* **132**, 1297–1304 (1986).
12. Lee, A. J. *et al.* Robust, linear correlations between growth rates and β-lactam–mediated lysis rates. *PNAS* **115**, 4069–4074 (2018).
13. Greulich, P., Scott, M., Evans, M. R. & Allen, R. J. Growth-dependent bacterial susceptibility to ribosome-targeting antibiotics. *Molecular Systems Biology* **11**, 796 (2015).
14. Lopatkin, A. J. *et al.* Bacterial metabolic state more accurately predicts antibiotic lethality than growth rate. *Nature Microbiology* **4**, 2109–2117 (2019).
15. Eng, R. H., Padberg, F. T., Smith, S. M., Tan, E. N. & Cherubin, C. E. Bactericidal effects of antibiotics on slowly growing and nongrowing bacteria. *Antimicrob Agents Chemother* **35**, 1824–1828 (1991).
16. Smirnova, G. V. & Oktyabrsky, O. N. Relationship between Escherichia coli growth rate and bacterial susceptibility to ciprofloxacin. *FEMS Microbiol Lett* **365**, (2018).
17. Levin, B. R. *et al.* A Numbers Game: Ribosome Densities, Bacterial Growth, and Antibiotic-Mediated Stasis and Death. *mBio* **8**, e02253-16 (2017).
18. Biselli, E., Schink, S. J. & Gerland, U. Slower growth of *Escherichia coli* leads to longer survival in carbon starvation due to a decrease in the maintenance rate. *Mol Syst Biol* **16**, (2020).
19. Roemhild, R., Bollenbach, T. & Andersson, D. I. The physiology and genetics of bacterial responses to antibiotic combinations. *Nat Rev Microbiol* (2022) doi:10.1038/s41579-022-00700-5.

20. Ocampo, P. S. *et al.* Antagonism between Bacteriostatic and Bactericidal Antibiotics Is Prevalent. *Antimicrobial Agents and Chemotherapy* **58**, 4573–4582 (2014).
21. Bollenbach, T., Quan, S., Chait, R. & Kishony, R. Nonoptimal microbial response to antibiotics underlies suppressive drug interactions. *Cell* **139**, 707–18 (2009).
22. Mitosch, K., Rieckh, G. & Bollenbach, T. Noisy Response to Antibiotic Stress Predicts Subsequent Single-Cell Survival in an Acidic Environment. *Cell Systems* **4**, 393-403.e5 (2017).
23. Hobbs, J. K. & Boraston, A. B. (p)ppGpp and the Stringent Response: An Emerging Threat to Antibiotic Therapy. *ACS Infectious Diseases* **5**, 1505–1517 (2019).
24. Poole, K. Stress responses as determinants of antimicrobial resistance in Gram-negative bacteria. *Trends in Microbiology* **20**, 227–234 (2012).
25. Schaechter, M., MaalØe, O. & Kjeldgaard, N. O. Dependency on Medium and Temperature of Cell Size and Chemical Composition during Balanced Growth of Salmonella typhimurium. *J Gen Microbiol* **19**, 592–606 (1958).
26. Ecker, R. E. & Schaechter, M. Ribosome content and the rate of growth of Salmonella typhimurium. *Biochimica et Biophysica Acta (BBA) - Specialized Section on Nucleic Acids and Related Subjects* **76**, 275–279 (1963).
27. Zaslaver, A. *et al.* Invariant distribution of promoter activities in Escherichia coli. *PLoS Comput Biol* **5**, e1000545 (2009).
28. Maaløe, O. & Kjeldgaard, N. O. *Control of Macromolecular Synthesis; a Study of DNA, RNA, and Protein Synthesis in Bacteria*. (W.A Benjamin INC, 1966).
29. Scott, M., Gunderson, C. W., Mateescu, E. M., Zhang, Z. & Hwa, T. Interdependence of Cell Growth and Gene Expression: Origins and Consequences. *Science* **330**, 1099–1102 (2010).
30. Hui, S. *et al.* Quantitative proteomic analysis reveals a simple strategy of global resource allocation in bacteria. *Molecular Systems Biology* **11**, (2015).
31. Kochanowski, K. *et al.* Global coordination of metabolic pathways in *Escherichia coli* by active and passive regulation. *Mol Syst Biol* **17**, (2021).
32. Mori, M. *et al.* From coarse to fine: the absolute *Escherichia coli* proteome under diverse growth conditions. *Mol Syst Biol* **17**, (2021).
33. You, C. *et al.* Coordination of bacterial proteome with metabolism by cyclic AMP signalling. *Nature* **500**, 301–6 (2013).
34. Towbin, B. D. *et al.* Optimality and sub-optimality in a bacterial growth law. *Nat Commun* **8**, 14123 (2017).
35. Palmer, A. C., Chait, R. & Kishony, R. Nonoptimal Gene Expression Creates Latent Potential for Antibiotic Resistance. *Molecular Biology and Evolution* (2018) doi:10.1093/molbev/msy163.
36. Brauner, A. & Balaban, N. Q. Quantitative biology of survival under antibiotic treatments. *Current Opinion in Microbiology* **64**, 139–145 (2021).
37. Yang, Y. *et al.* Temporal scaling of aging as an adaptive strategy of *Escherichia coli*. *Sci. Adv.* **5**, eaaw2069 (2019).
38. Hazan, R., Que, Y.-A., Maura, D. & Rahme, L. G. A method for high throughput determination of viable bacteria cell counts in 96-well plates. *BMC Microbiology* **12**, 259 (2012).
39. Sugino, A., Peebles, C. L., Kreuzer, K. N. & Cozzarelli, N. R. Mechanism of action of nalidixic acid: Purification of Escherichia coli nalA gene product and its relationship to DNA gyrase and a novel nicking-closing enzyme. *Proceedings of the National Academy of Sciences* **74**, 4767–4771 (1977).
40. Gellert, M., Mizuuchi, K., O'Dea, M. H. & Nash, H. A. DNA gyrase: an enzyme that introduces superhelical turns into DNA. *Proceedings of the National Academy of Sciences* **73**, 3872–3876 (1976).

41. Arnold, C. N., McElhanon, J., Lee, A., Leonhart, R. & Siegele, D. A. Global Analysis of *Escherichia coli* Gene Expression during the Acetate-Induced Acid Tolerance Response. *J Bacteriol* **183**, 2178–2186 (2001).
42. Kirkpatrick, C. *et al.* Acetate and Formate Stress: Opposite Responses in the Proteome of *Escherichia coli*. *J Bacteriol* **183**, 6466–6477 (2001).
43. Hengge, R. The General Stress Response in Gram-Negative Bacteria. in *Bacterial Stress Responses* (eds. Storz, G. & Hengge, R.) 251–289 (ASM Press, 2014). doi:10.1128/9781555816841.ch15.
44. Weber, H., Polen, T., Heuveling, J., Wendisch, V. F. & Hengge, R. Genome-Wide Analysis of the General Stress Response Network in Escherichia coli: σS-Dependent Genes, Promoters, and Sigma Factor Selectivity. *Journal of Bacteriology* **187**, 1591–1603 (2005).
45. Keren, L. *et al.* Promoters maintain their relative activity levels under different growth conditions. *Molecular systems biology* **9**, 701 (2013).
46. Gerosa, L., Kochanowski, K., Heinemann, M. & Sauer, U. Dissecting specific and global transcriptional regulation of bacterial gene expression. *Molecular systems biology* **9**, 658 (2013).
47. Dai, X. *et al.* Slowdown of Translational Elongation in Escherichia coli under Hyperosmotic Stress. *mBio* **9**, (2018).
48. Aidelberg, G. *et al.* Hierarchy of non-glucose sugars in Escherichia coli. *BMC Syst Biol* **8**, 1 (2014).
49. Nishino, K., Senda, Y. & Yamaguchi, A. CRP Regulator Modulates Multidrug Resistance of Escherichia coli by Repressing the mdtEF Multidrug Efflux Genes. *J Antibiot* **61**, 120–127 (2008).
50. Radzikowski, J. L. *et al.* Bacterial persistence is an active σ^S stress response to metabolic flux limitation. *Mol Syst Biol* **12**, 882 (2016).
51. Magnusson, L. U., Farewell, A. & Nyström, T. ppGpp: a global regulator in Escherichia coli. *Trends in Microbiology* **13**, 236–242 (2005).
52. Andersson, D. I. *et al.* Antibiotic resistance: turning evolutionary principles into clinical reality. *FEMS Microbiology Reviews* **44**, 171–188 (2020).
53. Baba, T. *et al.* Construction of Escherichia coli K-12 in-frame, single-gene knockout mutants: the Keio collection. *Molecular systems biology* **2**, 2006.0008 (2006).
54. Zaslaver, A. *et al.* A comprehensive library of fluorescent transcriptional reporters for Escherichia coli. *Nature Methods* **3**, 623–628 (2006).
55. Scrucca, L., Fop, M., Murphy, T., Brendan & Raftery, A., E. mclust 5: Clustering, Classification and Density Estimation Using Gaussian Finite Mixture Models. *The R Journal* **8**, 289 (2016).
56. Love, M. I., Huber, W. & Anders, S. Moderated estimation of fold change and dispersion for RNA-seq data with DESeq2. *Genome Biol* **15**, 550 (2014).
57. Mi, H. *et al.* PANTHER version 16: a revised family classification, tree-based classification tool, enhancer regions and extensive API. *Nucleic Acids Research* **49**, D394–D403 (2021).

Figures and figure legends.

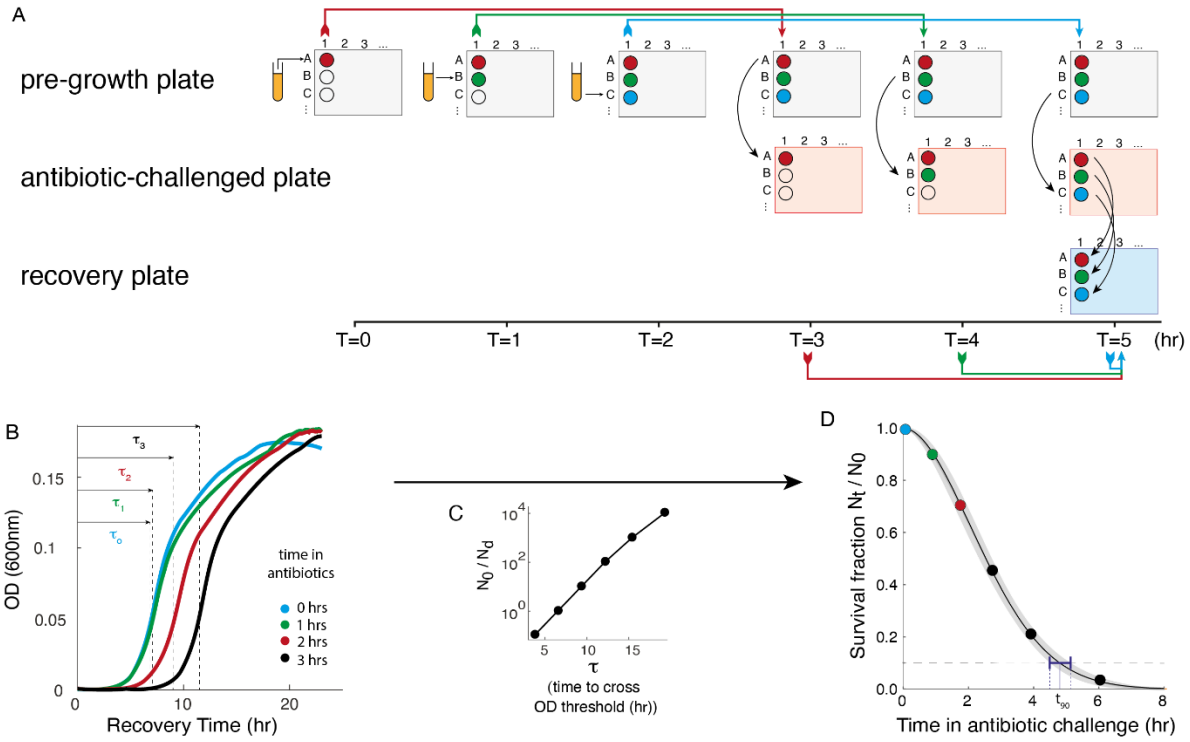

Fig 1. Death rate measurement protocol. For simplicity, we illustrate here the process for 3 time points (additional time points indicated in black) for a single growth condition, with 1 hr resolution. **A.** Scheme of the robotic process. (i) *Pre-growth*: in this stage bacteria are inoculated each hour in successive wells. (ii) *Antibiotic challenge*: after 3 hours of pre-growth, each exponentially growing culture is transferred to antibiotics. (iii) *Recovery*: all cultures are moved to antibiotic-free recovery medium at the same time, resulting in cultures that have been treated with antibiotics for various time durations. (i.e., wells in different colors have the same pre-growth conditions but spend different times in antibiotic) **B.** OD curves of cultures recovering from the antibiotic treatment. For each curve, we define the delay time τ to cross the OD=0.05 threshold indicated by the horizontal dashed line. Cultures that spent more time in antibiotics have larger τ. **C.** A standard curve obtained from the τ values of non-treated cultures with a range of dilutions ($N_0 =$ initial concentration, $N_d =$ diluted concentration) gives the relation between delay and relative number of bacteria. **D.** Surviving fraction as a function of time in the antibiotic challenge is calculated based on the measured τ and the standard curve ($N_0 =$ concentration of live cells at time 0, $N_t =$ concentration of live cells at time in antibiotic t). Based on at least 3 separate day repeats we obtained an average survival curve. We fit this curve with a Weibull survival function and defined death rate as 1/time for the function to drop to 10%. Error on the death rate was estimated by 95% confidence level of the fit.

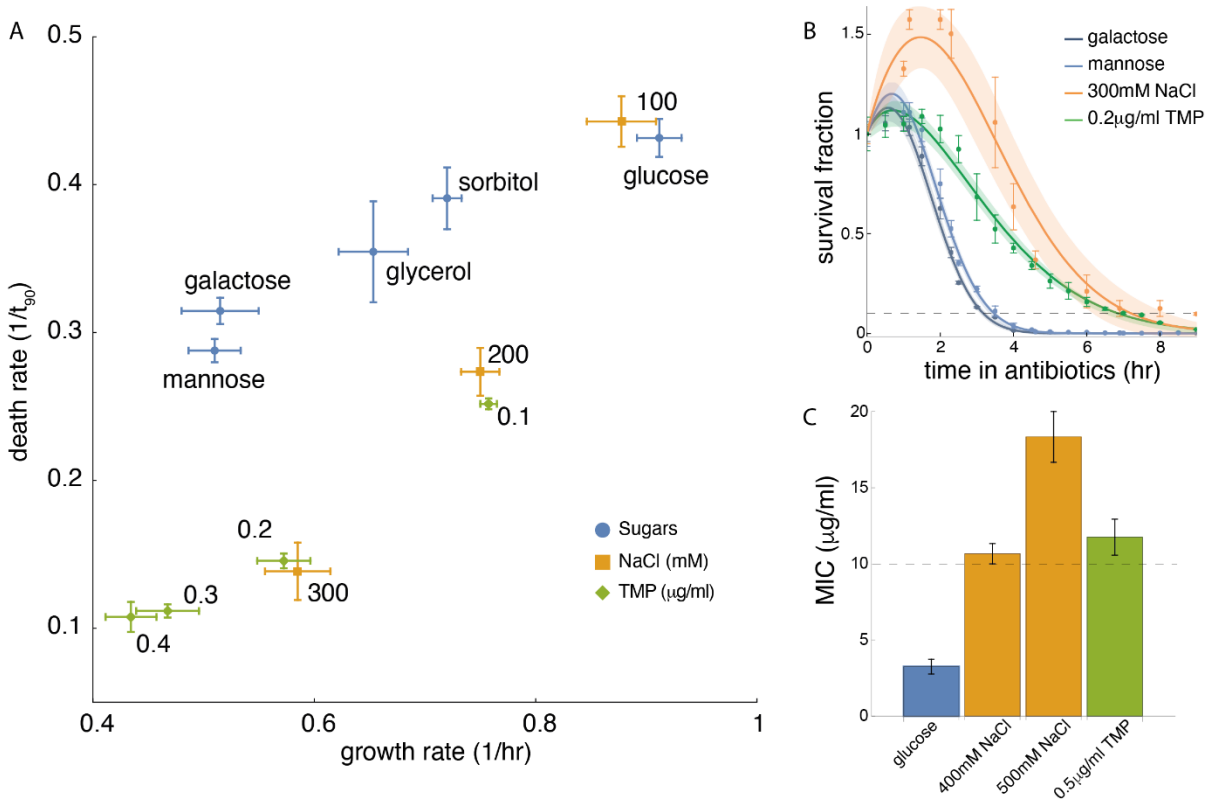

Fig 2. Antibiotic-mediated death depends on both growth rate and growth condition. **A.** The dependency of death rate on growth rate for NCM3722 strain (measured separately without nalidixic acid) under stress is steeper than under non-stressful conditions. Death rate upon treatment with 10 μg/ml nalidixic acid (determined as in Fig. 1) as a function of growth rate is shown for 12 different conditions (M9 + glucose as the reference point, M9 + 5 additional carbon sources and M9 + glucose + varying concentrations of NaCl or TMP). Each rate is determined based on 3 separate-day repeats. Error bars on the death rate are estimated by 95% confidence level of the survival curve and error bars on growth rate are standard error. **B.** At similar growth rates, stress conditions lead to lower death rates. Shown are survival curves for 4 different conditions with similar growth rate (0.52-0.59 1/hr), with shaded areas the 95% confidence interval of the fit (see Methods). For both NaCl and TMP, the survival curves show a slower decay compared to galactose and mannose, with a significant difference in the time to reach 10% survival (dashed line) used to determine the death rate. **C.** MIC increases for conditions with immeasurably low death rate. MIC is determined from growth curves in a range of antibiotic concentrations (methods). At high stress levels (>400 mM NaCl and 0.5 μg/ml TMP) the MIC is above 10 μg/ml nalidixic acid (the concentration used in panels A-B, dashed line). This is in line with our finding that the death rate under these stress conditions is below the detection level in our assay (Fig. S5).

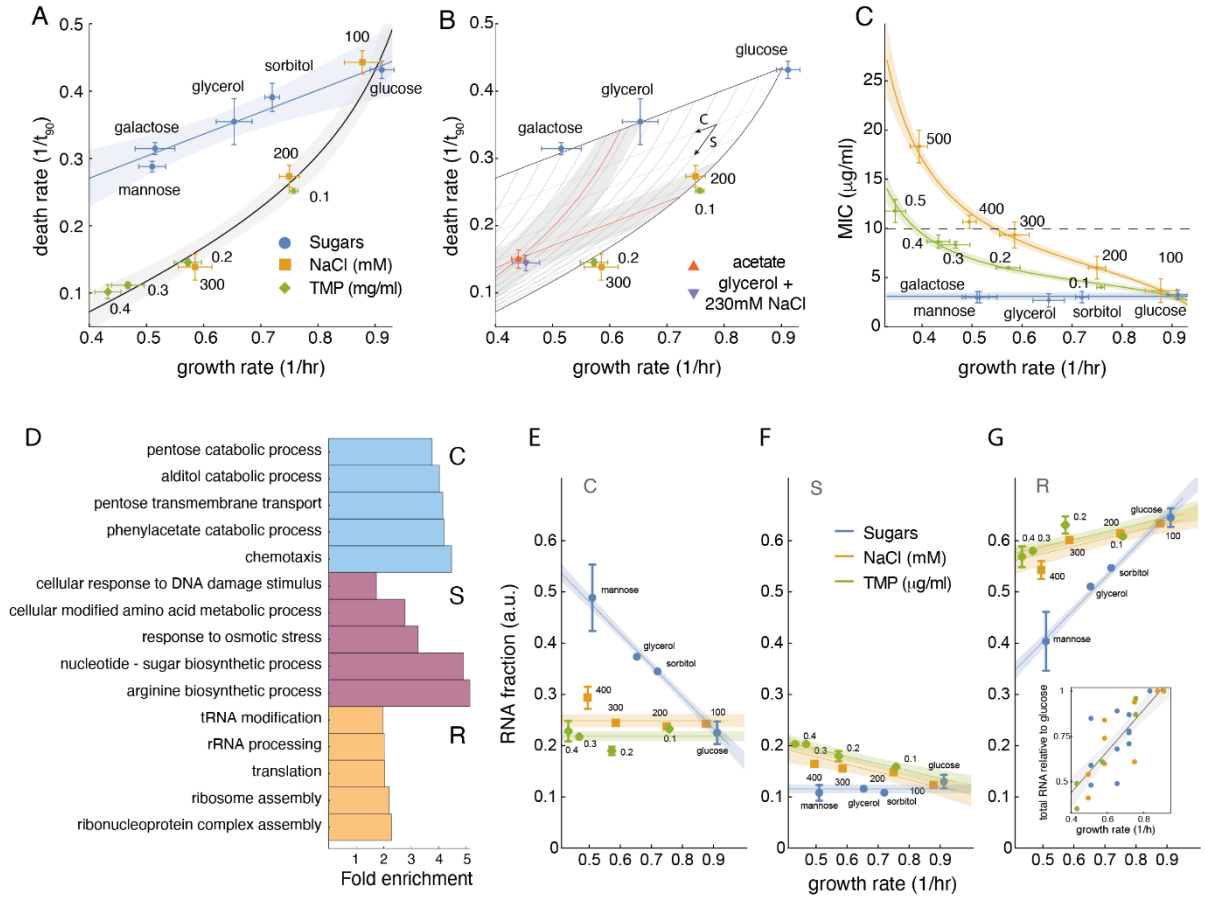

Fig. 3 A resource allocation model quantitatively matches growth, death, MIC, and sector measurements. **A.** Fitting Eqs 1-3 (see methods) to growth and death measurements from Fig. 2A produces a tight fit, with S constant for sugar data and C constant for stressors (blue line: fit for sugars, red curve: fit for stressors). **B.** The model maps a grid of C and S sector sizes one-to-one to growth and death rates (mostly horizontal lines: constant S, mostly vertical curves: constant C). Acetate (red point), which is both a carbon source and a stressor [41,42], lies between the sugar line and stress curve, and has growth and death rates that match quantitatively to predictions for a combination of glycerol and NaCl (purple point). **C.** The model also fits MIC data with the direct effect of growth on death (α) and the death rate on glucose (ρ_0 assumed to increase linearly with nalidixic acid concentration. **D.** Gene ontology (GO) terms for the determined C, S, and R sectors match expected behaviors of catabolism, stress, and growth, respectively. Displayed terms are 5 terms with lowest false discovery rate that are not child-terms of other significant terms. **E-G.** Total mRNA fraction of the measured sectors show that C is relatively constant with increasing stress while S is relatively constant regardless of sugar quality. R increases with growth rate, but at different slopes for sugars and stressors. **G inset.** Total RNA increases with growth rate at the same slope for both sugars and stressors. Shaded regions in all panels other than **B** are 90% confidence intervals on the fitted parameters. For **B** the error bands are propagated from the fits in **A** (see methods). See Table S2 for each fit's adjusted R^2 values.

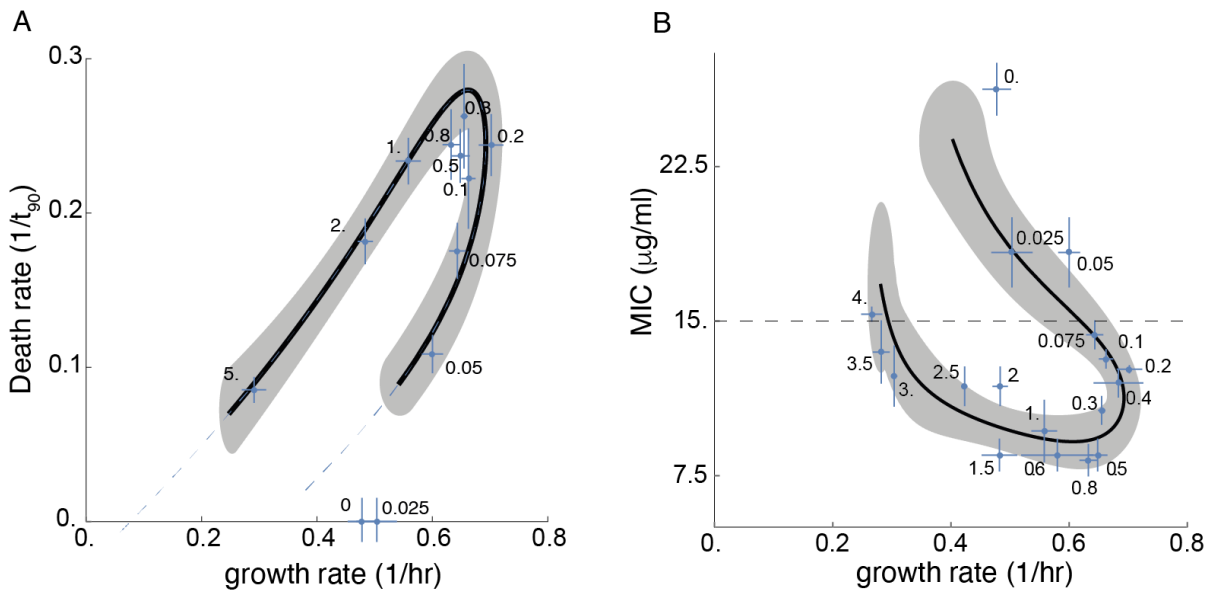

Fig. 4. The proposed resource allocation model quantitatively captures death rate, upon treatment with 15μg/ml nalidixic acid (**A)** and MIC (**B**) behavior as a function of cAMP in a ΔcyaA ΔcpdA strain. Shaded regions represent 90% confidence intervals on the fit. Points on the x-axis in **A** represent growth rates for conditions with immeasurably low rate; error in death rates for these points is taken to be the average error across all measured conditions. Horizontal dashed line in **B** is the concentration of nalidixic acid used in **A**. Note that the maximum growth rate in this strain differs from the wild type used in Figs 2-3. See Table S2 for the fit's adjusted R^2 value.

Methods

Strains. Experiments in this study were carried out using either NCM3722 strain (CGSC #12355) or MG1655 strain (CGSC #6300) and its derivatives MG1655ΔcyaA/ΔcpdA (U486[33]) and MG1655ΔrpoS, constructed by transducing the deletion from the Keio knockout collection [53] by P1 transduction. All strains were transformed with a kanamycin resistant, low copy promoterless plasmid (U66[53]) to acquire resistance and reduce contaminations during the long death experiments.

Growth rate and MIC measurements. Cells were grown overnight in M9 minimal medium (42mM Na_2HPO_4, 22mM KH_2PO_4, 8.5mM NaCl, 18.5mM NH_4Cl, 2mM $MgSO_4$, 0.1mM CaCl) containing 11mM glucose, 0.05% casamino acids and 50µg/ml kanamycin at 37°C and diluted 1:300 into the designated Media (all based on M9 with different carbon source, different concentration of NaCl etc.)

For growth rate measurements cultures were distributed using a robotic liquid handler (FreedomEvo, Tecan) in 96-well plates (150µl per well in at least 6 wells). Wells were covered with 100 µl of mineral oil (Sigma) to prevent evaporation and transferred into an automated incubator. Cells were grown in an automated incubator with shaking (6 hz) at 37°C for about 20 hours. Every 6-10 minutes the plate was transferred by a robotic arm into a multi-well fluorimeter (Infinite M200Pro, Tecan) that reads the bacteria optical density (OD, 600nm). For MIC measurements the setup was very similar with the following changes: cultures were pre-grown in tubes for 3-4 hrs and then distributed to wells containing different concentrations of Nalidixic acid.

Growth rate was calculated as the temporal derivative of the natural logarithm of the OD curves, $\mu = dln(OD)/dt$. Exponential growth rate is the mean over a region of at least 2 generations with a nearly constant growth rate.

MIC was determined as the minimal Nalidixic acid concentration which led to an OD decline (in NCM3722 strain, Fig. S6A) or a non-increasing OD curve (MG1655 strain, Fig. S6B).

Death rate measurements. A scheme of the experimental setup (carried out automatically in a robotic system (FreedomEvo, Tecan)) is shown in Fig 1 for one growth condition and a short experiment duration. In reality, in each experiment we measured 6-8 growth conditions and up to 16 hrs of antibiotic challenge.

This experimental setup contains 3 stages:

1. *Pre-growth stage*: This stage was carried out in a 96 well plate containing 200µl media (3-4 different growth conditions in a plate) +50µl mineral oil. As shown in Fig.1 an overnight culture (M9+11mM glucose+0.05% casamino acids+50µg/ml kanamycin) was diluted (1:300) into the growth plate. The culture was diluted to the first well of each condition (wells A1, A4, A7, A10 for a 4-conditions plate) and incubated in an automated incubator with shaking (6 hz) at 37°C for a time period (0.5-1 hr) which defines the experiment time resolution. Plates were transferred by the robotic arm into a multi-well fluorimeter (Infinite M200Pro, Tecan) that reads OD (600nm), followed by bacteria transfer from the overnight culture to the successive wells. This stage was repeated till the first well reached exponential phase (3-8 hrs, OD 0.02-

0.04).

2. *Antibiotic-challenge stage*: This stage was carried out in a 96 well plate containing 170µl media (same growth conditions as in the pre-growth plate+ Nalidixic acid) +50µl mineral oil). The first well of each condition of the pre-growth plate is diluted (1:7) into the antibiotic-challenged plate, in parallel inoculation of the ON culture to the pre-growth plate continues as well. Both plates are incubated with shaking (6 hz) at 37°C for the same time used in the pre-growth stage. Plates were transferred into a multi-well fluorimeter for OD measurements, followed by bacteria transfer to successive wells. For experiments with time resolution of 1 hr this stage was routinely repeated 16 times. For experiments with time resolution of 0.5 hr more repeats were carried out.
3. *Recovery stage*: In the last stage we adopted the protocol of Hazan *et. al*.[37] for viable cell determination based on the incubation time to cross a certain OD threshold. After the last transfer from the pre-growth plate to the challenged plate we immediately transferred the challenged plate to ice. Bacteria treated for different times as well as a non-treated culture were diluted 1:100 into 1 ml of recovery medium (M9+11mM glucose+50µg/ml kanamycin) in a deep 96-well plate. Non-treated cultures were also serially diluted in order to obtain a standard curve. Using the robotic system, we transferred each diluted culture to 6 wells of a 96-well plate (150µl per well). Wells were covered with 100 µl of mineral oil and transferred into an automated incubator. Cells were grown in an automated incubator with shaking (6 hz) at 37°C for about 20 hours. Every 10 minutes the plate was transferred by a robotic arm into a multi-well fluorimeter (Infinite M200Pro, Tecan) that reads the bacteria optical density (OD, 600nm). Setting the OD threshold to 0.05, $(\sim 2 \cdot background\ OD)$, we extracted from each OD curve the time (τ) required to reach this threshold (Fig1. B). Using the standard curve (Fig. 1C) we obtained for each growth condition the fraction of surviving bacteria as a function of antibiotic treatment time (Fig. 1D).
4. *Death rate calculation*: For each condition, we obtained an average survival curve based on at least 3 biological repeats (for the cAMP data we measured more cAMP levels with less repeats on each level). We fit the data with a Weibull survival function coupled to exponential growth, $e^{\mu t - \eta t^{\theta}}$, which allows fitting of exponential and sigmoidal survival curves as well as allowing for an initial increase in viable cells. For conditions in which the maximum occurred at 0 hr, we assumed $\mu = 0$ to ease fitting. To further ease the nonlinear fit, we restricted $\mu < 1$ (since growth rate without antibiotics are all below 1), $\eta > 1$ (at least exponential decay), that the maximum is below 2 and the time to reach the maximum is less than 2 hrs (well consistent with all data). We define death rate as 1/time for the fit to lose 90% of the population compared to the initial value at 0 hr. Error on the death rate was given by the 95% confidence level of the fit.

<u>RNA sequencing.</u> RNA was extracted from exponentially growing cultures using RNAeasy Protect bacteria Mini Kit (Qiagen). Total RNA was measured using Nanodrop (Thermo Scientific). For RNA sequencing rRNA was depleted using NEBNext rRNA depletion kit. RNAseq libraries were prepared at the Crown Genomics institute of the Nancy and Stephen Grand Israel National Center for Personalized Medicine, Weizmann Institute of Science. Libraries

were prepared using the INCPM-mRNA-seq without polyA selection protocol. Briefly, 80 ng of input RNA after ribosomal depletion was used for fragmentation and generation of double-stranded cDNA. After Agencourt Ampure XP beads cleanup (Beckman Coulter), end repair, A base addition, adapter ligation and PCR amplification steps were performed. Libraries were quantified by Qubit (Thermo fisher scientific) and TapeStation (Agilent). Sequencing was done on a Nextseq instrument (Illumina) using a 75 cycles high output kit. The Reads were mapped to the MG1655 genome. Expression levels for each gene were quantified using htseq-count.

RNA-Seq analysis and clustering. We acquired data for 4229 genes across all measured conditions, accounting for ~97% of *E. coli* genes. Because we sum gene expression to find sector sizes, we did not filter out low-read count genes. All raw count data was normalized using DeSeq2 after filtering out residual rRNA and tRNA reads. The Mclust [54,55] library was used to perform a Gaussian mixture model. Mclust recommended between 10 and 30 clusters with similar Bayesian Information Criterion (BIC) and spherical, unequal volume model ("VII"). We used the VII model with 12 clusters. The Spearman correlation for sugars, NaCl, and TMP conditions was subsequently calculated within each cluster, categorizing each line in each cluster as correlated, anticorrelated, or unchanging with growth rate. A liberal p-value cutoff of 0.2 for the correlation was used so as to include all genes as changing significantly in at least one set of conditions in at least one cluster. Clusters with only unchanging or positive correlations with growth rate were categorized as R. Clusters not in R and not anticorrelated with growth rate of the carbon sources were categorized as S. The remaining clusters were categorized as C, which included to some extent clusters increasing both in poor carbon sources and in increasing NaCl concentration.

Gene Ontology Analysis. Gene lists for each of the three sectors were checked for biological process gene ontology significance against the full list of E. coli genes using the rbioapi interface for PANTHER [56] using default parameters, including a significance cutoff of false discovery rate (FDR) below 0.05. The full list of GO terms and their significance are provided in Dataset S1. The terms displayed in Fig. 3D are those 5 terms with no significant encompassing terms with the lowest FDR.

Curve fitting. All fits in the paper were performed in Mathematica using NonlinearModelFit. For Fig. 3A, Eqs 1-3 were solved for death rate as a function of growth rate at either $C = C_0$ (stressors) or $S = S_0$(sugars), eliminated for R. This yielded the following prediction for death rate:

$$\text{Eq (4)} \quad \rho = \begin{cases} \rho_0 + \alpha(\mu - \mu_0) & \text{sugars} \\ \rho_0 + \alpha(\mu - \mu_0) - \beta \frac{\mu - \mu_0}{\mu - \mu_0 - ka} & \text{stressors} \end{cases}$$

Data was organized as 3-value points (type index, growth rate, death rate), with the index specifying the data point as sugar or stressor. These data were then fit to Eq. 4. Fitting weights were given as the inverse of the sum-square error of growth and death rates, with growth and death errors normalized first across all samples. Glucose was included as both a sugar and a stressor with half-weight each. The same procedure was followed in Fig. 3C and Fig. 3E-G.

For panel B, the one-to-one mapping between (C, S) to growth and death rates (μ, ρ) is provided by eliminating R from Eqs 1-3, yielding:

$$\text{Eq (5)} \quad \mu - \mu_0 = -a(C - C_0 + S - S_0)$$

$$\rho - \rho_0 = -a\alpha(C - C_0 + S - S_0) - \beta\frac{S-S_0}{k+S-S_0}$$

Or, vice versa:

Eq (6) $$C - C_0 = k - \frac{1}{a}(\mu - \mu_0) - k\frac{\beta}{\beta-\alpha(\mu-\mu_0)+\rho-\rho_0}$$

$$S - S_0 = -k + k\frac{\beta}{\beta-\alpha(\mu-\mu_0)+\rho-\rho_0}$$

In panel B, the spacing between successive curves of constant C or S assumed an arbitrary $a = 1$.

For panel C, we substituted $\alpha = \alpha_0(n - n_0)$ and $\rho_0 = \rho_{00}(n - n_0) = \mu_{00}\alpha$ in Eq. 4 as described in the main text. This yielded the following prediction for the MIC (n) when setting $\rho = 0$:

Eq (7) $$n = n_0 - \frac{\beta}{\alpha_0}\cdot\frac{(S-S_0)(\mu-\mu_0)}{((ka(C-C_0)+(S-S_0)(ka-\mu+\mu_0))(\mu-\mu_0+\mu_{00})} \ .$$

Upon substituting $S = S_0$ for sugars and $C = C_0$ for stressors, we arrive at

Eq (8) $$n = \begin{cases} n_0 & \text{sugars} \\ n_0 + \frac{\beta}{\alpha_0}\cdot\frac{\mu-\mu_0}{(\mu-\mu_0-ka)(\mu-\mu_0+\mu_{00})} & \text{stressors} \end{cases} \ .$$

Note that the constant value in sugars is not assumed upfront, but rather derives from the assumption that $S = S_0$ in sugars. The values for β, $k \cdot a$, and μ_0 were taken from the fit in Fig. 3A. The value of α_0 was allowed to differ for NaCl and TMP.

For panel E, a separate fit was performed for sugars, NaCl, and TMP. In each case, the data were fit to the expected piecewise linear function implied by Eq. 2:

Eq (9) $$\begin{aligned} R &= \frac{b}{a} + \frac{\mu}{a} \\ S &= S_0 \\ C &= 1 - \frac{b}{a} - S_0 - \frac{\mu}{a} \end{aligned} \qquad \text{sugars}$$

Eq (10) $$\begin{aligned} R &= \frac{b}{a} + \frac{\mu}{a} \\ S &= 1 - \frac{b}{a} - C_0 - \frac{\mu}{a} \\ C &= C_0 \end{aligned} \qquad \text{stressors}$$

where note that $b = aR_0 - \mu_0$.

All parameters matched within error (see supp. Table S1) except for a (as well as b, but yielding matching R_0, as described in the main text. The grid in Fig 3B was calculated by using the fits in Fig. 3A but with increasing values of C and S. The prediction lines through acetate were calculated by inverting the fit to find the C and S matching acetate. The error bands were calculated by propagating the error in the fit using AroundReplace.

For the relationship between total RNA and growth rate, we fit

Eq (11) $$\frac{r_{tot}}{r_{tot,0}} = a_{totRNA}\frac{\mu}{\mu_0} \ ,$$

where r_{tot} is the total RNA, $r_{tot,0}$ the total RNA in glucose growth, μ the growth rate, μ_0 the growth rate on glucose, and a_{totRNA} the fitted slope. We performed the fit for sugar, NaCl, and TMP conditions separately, as well as with all data combined.

For the fits to the cAMP data in Fig. 4, Eqs 1-3 were solved for death rate as a function

of growth rate and C. Growth rate was substituted with a [1/2]-order Padé approximant:

Eq (12) $$\mu = \frac{k_1 cAMP + k_2}{1 + k_3 cAMP + k_4 cAMP^2} \ ,$$

and C substituted as a Michaelis-Menten function of the C-sector data in Kochanowski, *et al.*[30]:

Eq (13) $$C = \nu_0 + \nu_{max} \frac{cAMP}{\kappa + cAMP} \ .$$

These two functions were fit independently, with weights given by the inverse error of the growth rates in the case of fitting Eq 12.

Solving for the death rate, and using, we find that

Eq (14) $$\rho = \rho_0 + \alpha(\mu - \mu_0) + \beta \frac{ka}{ka + a(C - C_0) + \mu_0 - \mu} \ .$$

With $\alpha = \alpha_0(n - n_0)$ and ρ_0 linear functions of nalidixic acid concentration as described in the main text, the MIC is

Eq (15) $$n = n_0 + \frac{\beta}{\alpha_0} \cdot \frac{\mu - \mu_0 + a(C - C_0)}{(\mu - \mu_0 - ka + a(C - C_0))(\mu - \mu_0 + \mu_{00})} \ .$$

We fit Eqs. 13 – 14 (with μ and c replaced with Eqs. 12 and 13, respectively) simultaneously by setting $\alpha = \alpha_0(n_{15} - n_0)$ in Eq 14 (thus exchanging the parameter α for n_{15} and using a combined set of points {index, cAMP, death rate} and {index, cAMP, MIC} from Figs. 4A-B with index indicating the type of point (death rate or MIC). These points were fit to a piecewise function equal to Eq 14 for death rate points Eq 15 for MIC points. The parameters μ_0 was taken as the average of points with growth rate above 0.65 / h (near the glucose optimum) and c_0 taken as the fitted size of the C sector from Eq. 13 at the average cAMP concentration of the averaged points. The value of $k \cdot a$ was not fit well, and as such was simply assumed to be the same as the fit in Fig. 3A. Fitting weights were given as the inverse of the error in the death rates and MICs, normalized by the mean of all death rates and MICs, respectively.

Code availability

RNA-Seq analysis was performed in R version 4.1.0. All other fitting and analytical manipulation were performed in Mathematica version 13. Source code can be found in Dataset S2.

Data availability

All data not provided in the text or supplements is available upon request.

Acknowledgements

We thank B. Towbin, S. Kostinski, T. Milo, A. Bar, Y. Yang, and E. Vaisbourd for comments on the manuscript. Funding was provided by European Research Council (ERC) under the European Union's Horizon 2020 research and innovation program (grant agreement No. 856587). D.S.G. was funded as a member of the Zuckerman Postdoctoral Scholars Program. U.A is the incumbent of the Abisch-Frenkel Professional Chair.

Author contributions

A.B. conducted experiments and analysis. A.M. and D.S.G. performed theoretical analysis and fits. All authors contributed to conception and to writing of the manuscript.

Competing interests

The authors declare no competing interests.

Supplementary information

Supplementary Figs. S1-S11 and Tables S1-S2 are provided in the supplementary information.